PNAS RESEARCH ARTICLE | Physical Sciences

Near-total loss of buttressing stresses observed on Pine Island Ice Shelf, West Antarctica

Sarah Wells-Moran[a,b,1], Brent Minchew[c,b], and Bryan Riel[d]

This manuscript was compiled on January 26, 2026

Ice shelves, the floating extensions of the Antarctic Ice Sheet, provide critical buttressing stresses that resist the seaward flow of ice and help set the position of the grounding line, where the ice goes afloat. As buttressing stresses are diminished by thinning or fracturing and collapse of the ice shelf, glaciers tend to accelerate. Here, we focus on the response of Pine Island Ice Shelf (PIIS) in West Antarctica to multiple calving events and the disintegration of the lateral shear margins. Using observed time-series of the surface velocity fields between 2015 and 2024, we show multiple episodes of acceleration in ice flow and a marked reduction in the buttressing stresses. These observations show that PIIS experienced an near-total loss of its buttressing capacity during the observational record. We then investigate how a model glacier responds to loss in margin buttressing, and are able to broadly reproduce observations. By linking model outputs to observations, we recreate a timeline of buttressing loss on PIIS. These losses likely foreshadow a period of grounding line retreat and acceleration of Pine Island Glacier's contribution to global mean sea level rise.

Buttressing | Ice Shelf | Collapse | Pine Island Glacier

Antarctic ice shelves – the floating extensions of the ice sheet – provide critical "safety bands" around the continent that moderate the flux of ice mass into the ocean through the buttressing effect they provide (1–3). When the Larsen B Ice Shelf collapsed in 2002, the glaciers buttressed by the shelf sped up two-to-six fold (4–6), emphasizing the important stabilizing role ice shelves play in ice sheet mass loss. Buttressing forces are especially important for the stability of the West Antarctic Ice Sheet (WAIS), which holds 5.3 m of sea level equivalent (7), as buttressing enables a marine ice sheet grounded on a retrograde bed, such as WAIS, to have a stable grounding line that would otherwise be vulnerable to rapid retreat in response to perturbations (2, 8). Despite the important role ice shelves play in modulating rates of sea level rise, the processes that control ice shelf stability and collapse are poorly understood due largely to a lack of observations, as only a handful of ice shelves have collapsed in the observational record (9–11). The lack of understanding about the future stability of the Antarctic ice shelf "safety bands" contributes significant uncertainty to sea level rise projections (12, 13).

We aim to disentangle the processes that contribute to loss of buttressing by investigating nearly a decade of observations over Pine Island Glacier as it has evolved in response to increasing ice damage. Pine Island Glacier (PIG) is the fastest flowing glacier in Antarctica (14) and is the largest contributor to sea level rise of all Antarctic glaciers (7, 15, 16). The Pine Island Ice Shelf (PIIS) buttresses 51 cm of sea level equivalent (7) and the glacier is grounded on a retrograde slope (17), leaving it vulnerable to irreversible retreat in response to perturbations. Between 1973 and 2013, ice discharge from PIG increased by 77%, with ice shelf velocities increasing from 2.2 km/yr in 1974 (18) to 4 km/yr by 2008 and increases in ice velocity detected throughout almost the entire PIG drainage area (19). Between 2008 and 2017, velocities on the ice shelf remained relatively stable at approximately 4 km/yr, followed by another period of acceleration between 2017 and 2023, where ice shelf velocities further increased to 4.8 km/yr, a 20% increase over 6 years (20) and a 113% increase since 1973. Increased ice velocity is often accompanied by grounding

Significance

Ice shelves provide a key source of stability to the Antarctic Ice Sheet by buttressing the flow of grounded ice. As ice shelves weaken and collapse due to rising temperatures, the glaciers buttressed by them speed up, increasing Antarctica's contribution to sea level rise. Pine Island Glacier is the fastest flowing glacier in Antarctica and the ice shelf that buttresses it has undergone significant change in the last decade, resulting in a 20% increase in ice velocity. We compare observations to models to better understand the processes contributing to buttressing loss in ice shelves and conclude the Pine Island Ice Shelf now provides negligible buttressing to the ice upstream, destabilizing the grounding line and accelerating mass loss from West Antarctica.

Author affiliations: [a]Department of Geophysical Sciences, University of Chicago, Chicago, IL 60615; [b]Department of Earth, Atmospheric, and Planetary Sciences, Massachusetts Institute of Technology, Cambridge, MA 02139; [c]Seismological Laboratory, California Institute of Technology, Pasadena, CA 91125; [d]School of Earth Sciences, Zhejiang University, Hangzhou, P.R. China 310058

The authors worked together to conceive and design the project. This work was completed as part of S.W.M.'s Masters thesis. S.W.M. analyzed the data, conducted model simulations, generated figures, and wrote the first draft of the manuscript. B.M.M. supervised the project, assisted with data analysis, and contributed sections to the manuscript. B.V.R. generated the strain rate fields and assisted with data analysis. All coauthors contributed to the revision of the manuscript.

All authors declare no financial, personal, nor professional conflicts of interest. Disclosure: BMM is a co-founder of Arête Glacier Initiative (areteglaciers.org), where he serves as Chief Scientist through his allowance for outside professional activities provided by Caltech (current affiliation) and MIT (past affiliation). Arête is a non-profit organization that is currently a fiscally sponsored project of the Digital Harbor Foundation, a 401(c) 3. Arête was founded in 2024 to provide funding for glaciological research focused on forecasting and slowing sea-level rise. No funding was provided by Arête for this work.

[1]To whom correspondence should be addressed. E-mail: swellsmo@uchicago.edu

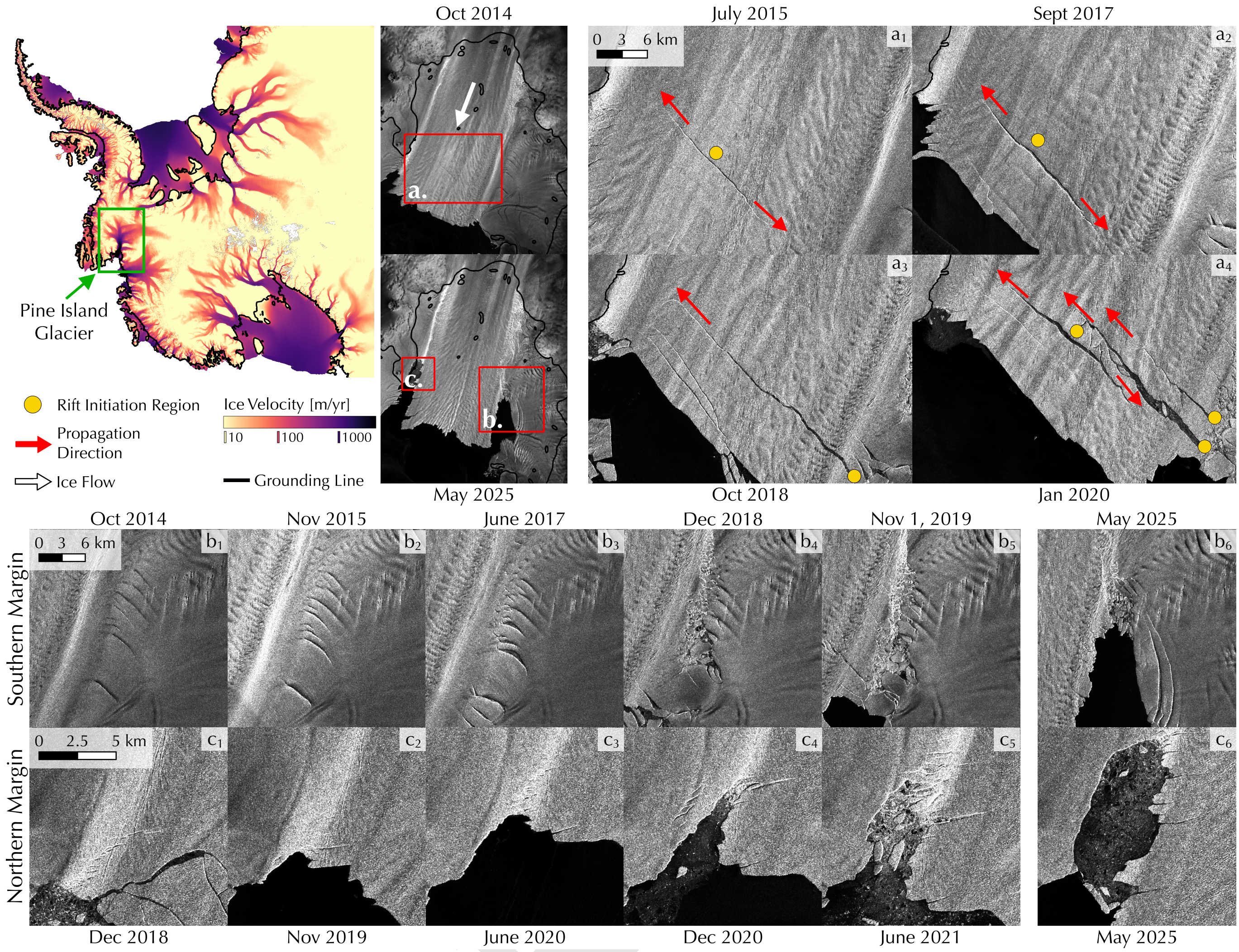

Fig. 1. (top left) The location of Pine Island Glacier (PIG) on Antarctic ice velocity map (29). Below, Sentinel-1 images show the full extent of the Pine Island Ice Shelf (PIIS) in 2014 and 2025 with direction of flow denoted by a white arrow and the extents of (a-c) boxed in red. (a) Modified Copernicus Sentinel-1 images of the PIIS prior to each of the four observed calving events. The approximate area of rift initiation is denoted as a yellow circle, and the direction of rift propagation is noted with red arrows. Rifts (a_1) $\mathbf{C}_{2015}$ and (a_2) $\mathbf{C}_{2017}$ initiate in the center of the ice shelf and propagate laterally outwards as they advect downstream. A change in calving styles then occurs, with (a_3) rift $\mathbf{C}_{2018}$ initiating in the Southern Shear Margin (SSM) and propagating across flow towards the Northern Shear Margin (NSM). (a_4) Rift $\mathbf{C}_{2020}$ initiates in the center of the ice shelf and propagates outwards towards the margins as it advects downstream, and is later joined by two rifts initiating from the SSM. (b,c) Increasing damage and disintegration of the SSM and NSM as seen in Sentinel 1 imagery. ($b_{4,5}$) and (c_{4-5}) show rapid fragmentation in the SSM and NSM following $\mathbf{C}_{2017}$ and $\mathbf{C}_{2020}$, respectively. (b_6, c_6) The state of the SSM and NSM as of May 9th, 2025.

line retreat as the glacier thins to accommodate the increase in ice flux (3). Between 1992 and 2011, the PIG grounding line retreated more than 31 km (21–23). These increases in ice shelf velocity are likely closely linked to loss of buttressing through a variety of processes, including increased basal melt (24, 25), dynamic thinning, calving (20), and damage evolution (26–28).

Past and Present Observations of Damage on PIIS

We primarily focus on damage development and evolution as a mechanism for buttressing loss, motivated by current observations of increasing damage in the PIIS Southern margin (28, 30) and historical records over PIIS of a cyclical process of increasing margin damage leading to calving front retreat dating back as far as 1972 (31). The processes that control damage formation and evolution are poorly constrained in natural glacier ice (32–35), but the effects of damage on the bulk material properties of ice are relatively well understood. As damage increases, the bulk viscosity of the ice decreases (36–38), causing areas that previously supplied a back stress on the ice shelf, such as shear margins or pinning points, to provide less resistance to flow, decreasing the buttressing force imposed by the ice shelf on the grounded ice upstream. We build on the previous literature by expanding the analysis of the observational record over PIG to 2025 and linking observations to idealized model responses to decreased margin viscosity as a proxy for increased damage and use these comparisons to create a timeline of buttressing loss on the PIIS over the last decade.

We investigate changes in visible damage on PIIS between January 2015 and February 2024 using Sentinel-1A and 1B imagery. We observe four calving events in this time period: $\mathbf{C}_{2015}$ calves between July 25th and August 6th, 2015; $\mathbf{C}_{2017}$ between September 21st and 23rd, 2017; $\mathbf{C}_{2018}$ between October 25th and 29th, 2018; and $\mathbf{C}_{2020}$ between February 7th and 9th, 2020 (Fig. 1a). The rifts that form $\mathbf{C}_{2015}$ and $\mathbf{C}_{2017}$ initiate in the center of the ice shelf, likely as basal crevasses (39), and propagate outward on both sides as the rifts advect downstream. We then observe a change in rifting styles, indicating a shift in stress states across the ice shelf. The $\mathbf{C}_{2018}$ rift initiates from the SSM and rapidly propagates across-flow towards the NSM. The calving style further changes for $\mathbf{C}_{2020}$. Similarly to $\mathbf{C}_{2015}$ and $\mathbf{C}_{2017}$, the primary $\mathbf{C}_{2020}$ rift initiates in the center of the ice shelf around 2017 and propagates outward as it advects downstream. As the initial $\mathbf{C}_{2020}$ rift approaches the calving front, two rifts initiate in the SSM and propagate North towards the initial rift, creating a complex rift system that eventually forms $\mathbf{C}_{2020}$. As of November 2025, no further calving events have occurred. In addition to the observed calving events, we see an increase in damage, defined as visible crevasses and melange, in both shear margins (Fig. 1 b,c). Between 2015 and 2017, existing rifts in the SSM slowly widen. After $\mathbf{C}_{2017}$, the rifts connect and the margin quickly deteriorates into melange, which is then evacuated from the area, leaving open water. Shortly after $\mathbf{C}_{2020}$, the NSM, which does not have an existing crevasse field, undergoes a similar rapid disintegration. Additionally, the lower trunk of the glacier swings southward as it loses contact with the PIG Southern Ice Shelf.

Response of PIIS to Increasing Damage

We aim to link visible changes in ice shelf damage to observable changes in velocity and strain rates. We develop 1000 time-dependent velocity fields with a time step of ~ 3 days (see 0.1) over PIG from January 2015 to 2024 and from the velocities derive effective and principal strain rate fields, following the convention of $\dot{\epsilon}_1 > \dot{\epsilon}_2$ and positive values denoting tension. Thus, the ice shelf is in a purely tensile regime when $\dot{\epsilon}_2 > 0$ as $\dot{\epsilon}_1$ must necessarily be positive by convention. For this reason, we analyze changes in tensile regimes on the ice shelf via the least principal strain rate $\dot{\epsilon}_2$. For each field, we calculate mean, minimum, and maximum velocities and strain rates within a 156.25 km^2 area (51 x 51 pixels) in the center of the ice shelf, outlined in Fig. 2a$_1$, which we use to represent the average state of the ice shelf.

The mean velocity of the ice shelf increases by almost 900 m/yr between 2015 and 2024, the majority of which occurs between 2017 and 2022. The ice shelf begins speeding up in April 2017, 5 months prior to $\mathbf{C}_{2017}$, and begins slowing down after March 2022. Velocities increase again in February 2023 and continue increasing through the end of our observational data. The maximum rate of acceleration occurs around April 2020, two months after $\mathbf{C}_{2020}$, and the next two largest accelerations occur one month after $\mathbf{C}_{2018}$ and three months after $\mathbf{C}_{2017}$, respectively. The 900 m/yr speed up does not occur uniformly across flow (Fig. 3). The 2017 speed up initiates in the SSM close to the calving front, and increased velocities propagate diagonally towards the region of the NSM close to the grounding line. After $\mathbf{C}_{2018}$, a velocity wave propagates outwards from the NSM and laterally across the ice shelf. The third major velocity increase initiates from the downstream NSM in 2020. Part of this velocity increase is a continuation of the increase associated with $\mathbf{C}_{2018}$, which $\mathbf{C}_{2020}$ accentuates and accelerates. Each calving event causes a larger velocity increase than the previous event in the 132 days between panels (1) and (5) in Fig. 3.

The SSM migrates 5-10 km outward from the trunk of the ice shelf between 2015 and 2018 (Fig S3), a similar time period to the observed increase in damage and weakening within the margin, which has been noted in other studies (30). To better visualize changes in strain rates, we subtract the January 2015 $\dot{\epsilon}_E$ field from subsequent $\dot{\epsilon}_E$ fields and refer to the resulting fields as $\Delta\dot{\epsilon}_E$. In $\Delta\dot{\epsilon}_E$, we observe a distinctive pattern associated with margin weakening. As damage within the margin increases, bulk viscosity decreases, resulting in a steeper velocity gradient concentrated through damaged areas. The shear margin follows the path of lowest viscosity, and either migrates towards regions of damage (SSM) or narrows as damage increases within the margin (NSM). In $\Delta\dot{\epsilon}_E$ fields, this weakening pattern is reflected as bands of decreasing $\dot{\epsilon}_E$ where the original margin was located directly adjacent to bands of increasing $\dot{\epsilon}_E$ where damage exists (Fig 2b$_2$). This weakening pattern is visible in the SSM throughout the entire observational record and clearly captures the outward migration of the margin. In the NSM, a weak region is visible as early as 2015 towards the PIG grounding line (Fig. S3). After $\mathbf{C}_{2015}$, a weak region appears towards the calving front on the NSM. Both regions extend towards each other along the NSM until they join in 2018, indicating weakening along the entire margin (Fig S4).

In contrast to the increase in ice velocity, which starts in 2017 and continues increasing at a relatively consistent rate, we observe two distinct periods of increasing strain rates (Fig. 2c). Between $\mathbf{C}_{2017}$ and $\mathbf{C}_{2020}$, both principal and effective strain rates gradually increase. After $\mathbf{C}_{2020}$, strain rates sharply increase, and then level out around January 2021 before starting to decrease in December 2021. The maximum rate of increase in both velocity and strain rates occurs in close proximity to $\mathbf{C}_{2020}$ (Fig. S1, S2). After $\mathbf{C}_{2020}$, the ice shelf shifts to an almost entirely tensile regime, defined by $\dot{\epsilon}_1, \dot{\epsilon}_2 > 0$ (Fig. 2a$_3$,b$_3$,d). Prior to $\mathbf{C}_{2020}$, between 25% and 50% of $\dot{\epsilon}_2$ values sampled are negative and the mean of $\dot{\epsilon}_2$ is 1.3×10^{-3} yr^{-1}, whereas after $\mathbf{C}_{2020}$, less than 25% of sampled $\dot{\epsilon}_2$ are negative and the mean of $\dot{\epsilon}_2$ more than quadruples to 5.8×10^{-3} yr^{-1} (Fig. 2d).

To better contextualize these observations of change on PIIS, we investigate the response of a simple model ice shelf to induced margin damage. We utilize the Ice-Sheet and Sea-level System Model (ISSM) (42) and spin up an idealized glacier to steady state following the MISMIP+ geometry, methodology, and parameters (43), which is qualitatively based on PIG. Once the model reaches steady state, we simulate damage in the ice shelf margin by decreasing the ice viscosity coefficient (rigidity parameter) by an order of magnitude and then calculate the instantaneous stress response of the model to the imposed damage. We investigate two scenarios of buttressing loss via induced damage: 1) Damaging the downstream edge of one model margin, and 2) damaging both margins. The region of imposed damage for both scenarios is outlined in green on Fig. 4 b$_1$ and c$_1$, respectively.

Similarly to our analysis of the observations, we subtract steady state (Fig. 4a) from modeled instantaneous changes in velocity and $\dot{\epsilon}_E$. In both model scenarios,

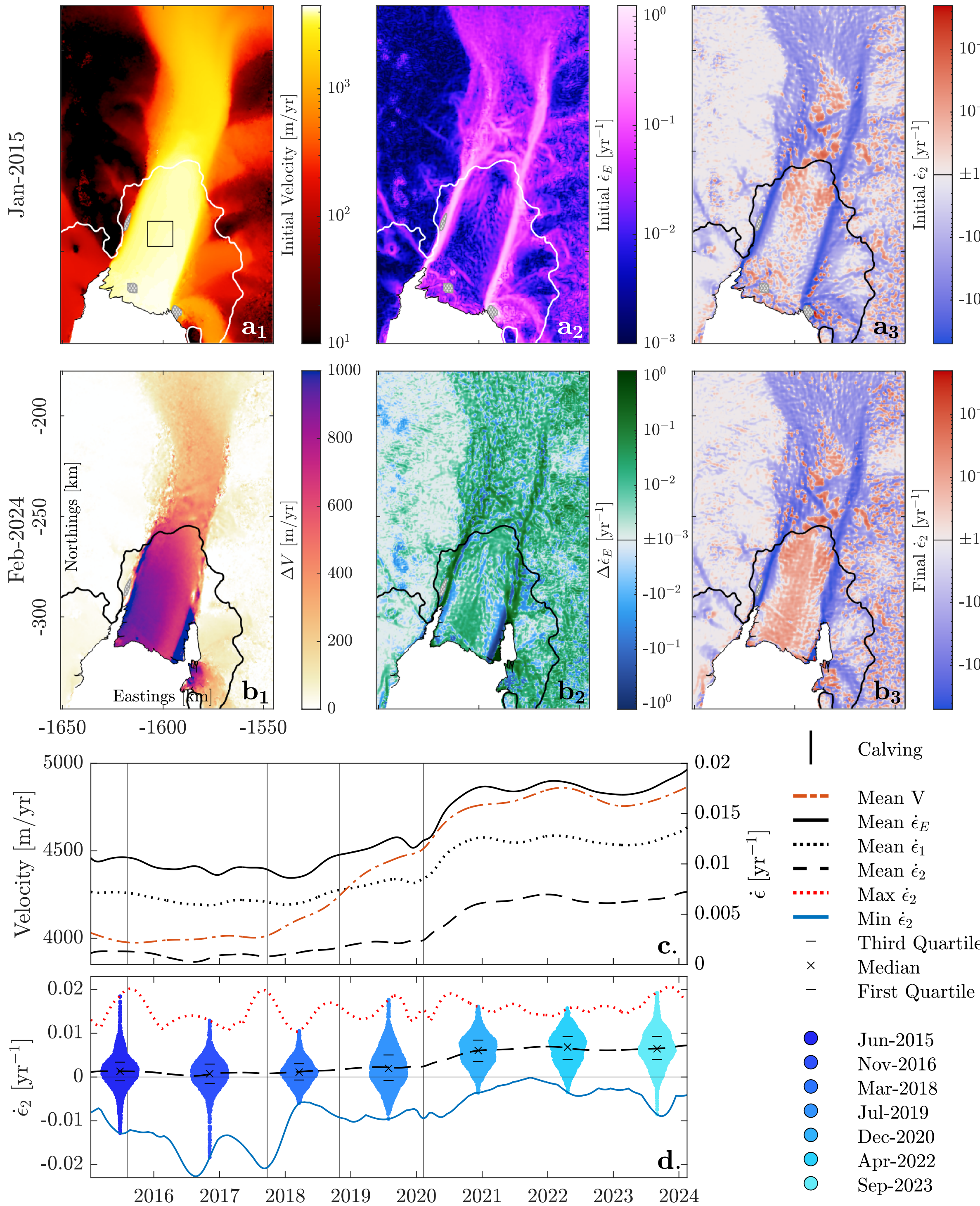

Fig. 2. The evolution of observed velocity and strain rate fields on PIG between January 2015 and February 2024. (a_1) Velocity, (a_2) effective strain rate ($\dot{\epsilon}_E$), and (a_3) least principal strain rate ($\dot{\epsilon}_2$) fields from January 2015. Change in (b_1) velocity and (b_2) $\dot{\epsilon}_E$ in February 2024 relative to (a_1) and (a_2), respectively. (b_3) $\dot{\epsilon}_2$ in February 2024, showing a widespread increase in purely tensile regions across the ice shelf. All data in (a,b) are overlain with grounding lines from (40, 41), and patches of no data are covered with hatched blobs. We select a 12.75 km^2 area, boxed in black in (a_1), over which we sample values of velocity and strain rates that are representative of average values across the ice shelf. We plot sampled (c) mean velocity (orange) and mean effective, least, and maximum strain rates (black) and (d) maximum, mean, and minimum values of $\dot{\epsilon}_2$ from 2015 to 2024. Black vertical lines denote calving dates. Additionally, in (d) we plot the distribution of all sampled $\dot{\epsilon}_2$ at 7 dates, with width of point scatter denoting the density of points with similar values. 50% of the sampled points are located between the horizontal quartile lines for each date. After $\mathbf{C}_{2020}$, more than 75% of the sampled $\dot{\epsilon}_2$ values are greater than 0.

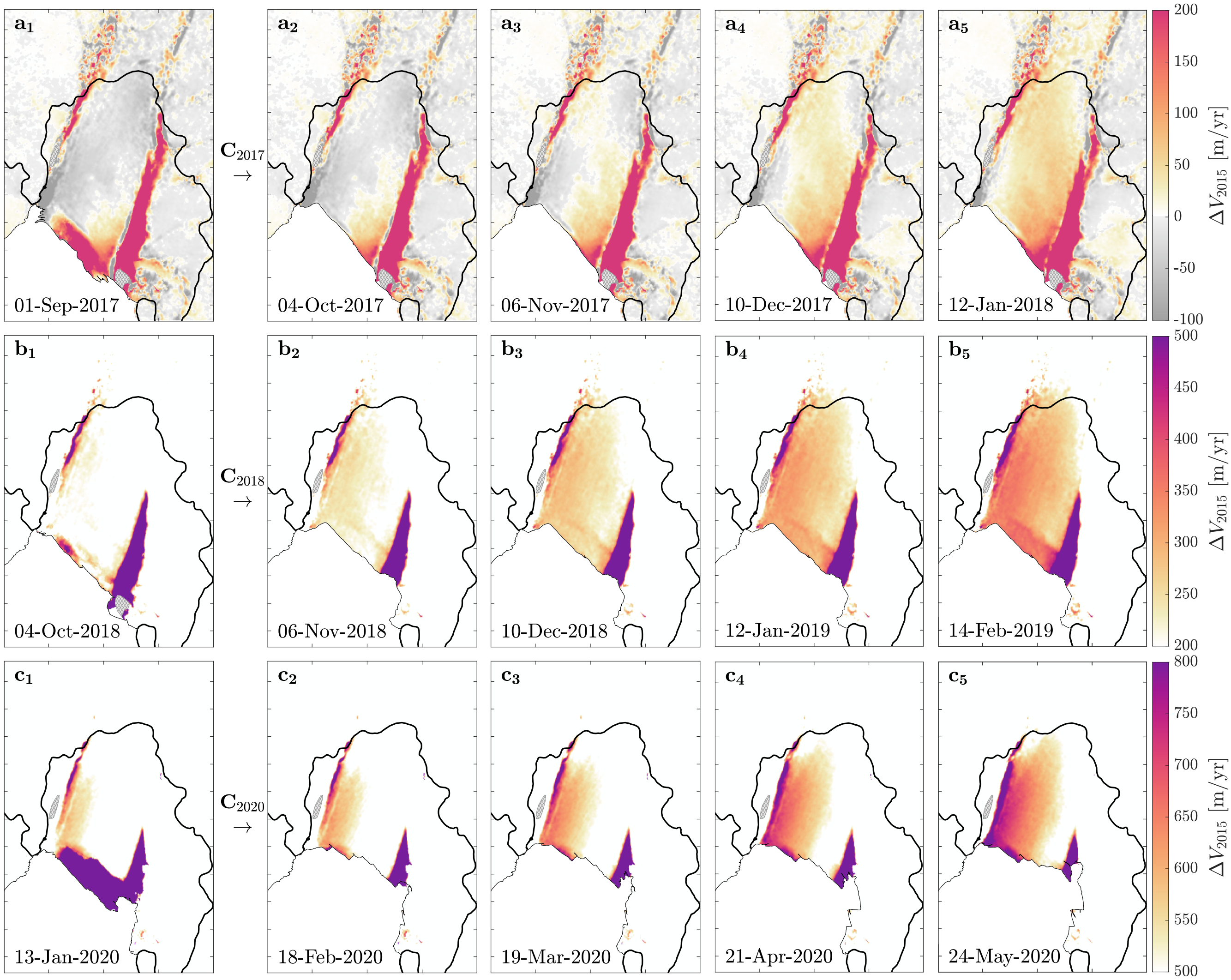

Fig. 3. Change in ice shelf velocity (1) preceding and (2-5) directly after (a) $\mathbf{C}_{2017}$, (b) $\mathbf{C}_{2018}$, and (c) $\mathbf{C}_{2020}$ at time steps of approximately 33 days. Colorbars are in reference to January 2015 and start at different values of ΔV with a total span of 300 m/yr, allowing for better visualization of smaller across-flow velocity changes closely correlated to calving events. After $\mathbf{C}_{2017}$, increased velocities propagate from the downstream edge of the SSM towards the upstream portion of the NSM. After $\mathbf{C}_{2018}$ and $\mathbf{C}_{2020}$, increased velocities propagate across flow from the NSM towards the SSM. Average velocities on the ice shelf increase by approximately (a) 65 m/yr, (b) 125 m/yr, and (c) 152 m/yr in the 132 days between (1) and (5). Grounding lines are from 2022 (40, 41) and we manually trace the ice front location from Sentinel-1 imagery.

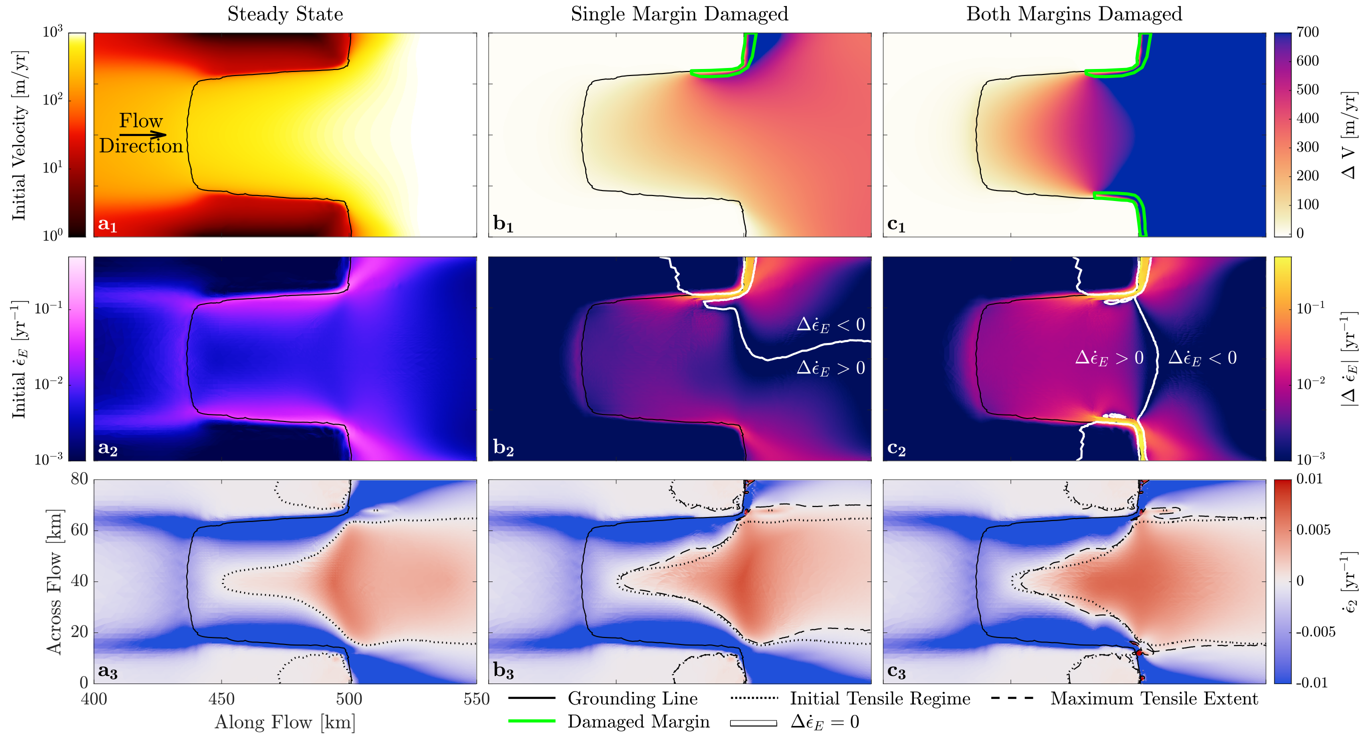

Fig. 4. Ice sheet model results for (a) the steady state glacier after model spin up, (b) the instantaneous stress response after weakening a single margin, and (c) the instantaneous stress response after weakening both margins. (b_1) and (c_1) show changes in modeled velocity relative to (a_1), with the area of weakened margin outlined in green. (b_2) and (c_2) show changes in the magnitude of modeled effective strain rate relative to (a_2), with a solid white line separating regions of increasing and decreasing strain rates relative to (a2) steady state. (b_3) and (c_3) show the modeled $\dot{\epsilon}_2$ field, with red denoting areas in pure tension ($\dot{\epsilon}_1, \dot{\epsilon}_2, > 0$). The steady state tensile extent is plotted as a dotted line on both (b_3) and (c_3) to better visualize change in tensile extent between each scenario.

we observe a large increase in $\dot{\epsilon}_E$ within the damaged margin and a decrease in $\dot{\epsilon}_E$ directly adjacent to the damaged margin. When only one margin is damaged, strain rates also increase on the downstream corner of the opposite, intact margin (Fig 4b_2). Additionally, in the single margin scenario, instantaneous velocity increases across flow and the region of pure tension expands towards the damaged margin. When both margins are damaged, velocity increases symmetrically across flow and the largest increase in velocity is along the center line, and the region of the model in pure tension widens to encompass a larger area in the center of the ice shelf.

Reconstructing a Timeline of Buttressing Loss

We compare model outputs to observed changes on PIIS to construct a timeline of buttressing loss (Fig. 5). Between 2015 and 2024, the majority of buttressing is lost via the ice shelf decoupling from its shear margins, primarily via damage development and secondarily through calving. Damage is present in the SSM prior to 2015 and increases over time (Fig. 1b), thus limiting the ability of the margin to resist ice flow. As seen in both models (Fig 4b,c) and observations (Fig. 2b_2), effective strain rates increase within damaged regions, which promotes further damage development and weakening. $\mathbf{C}_{2017}$ then removes a portion of ice along the SSM that was providing crucial lateral compression to stabilize the ice shelf. After this keystone piece of ice calves, the SSM rapidly fractures into melange (Fig. 1$b_{4,5,6}$). Models show a significant speed up originating from the decoupled region, which we observe occurring directly correlated with $\mathbf{C}_{2017}$ (Fig 3a). $\mathbf{C}_{2017}$ marks the start of the 20% increase in observed velocities over a period of 5 years.

As the SSM decouples from the trunk of the ice shelf, velocities near the SSM increase and induce rotation about the downstream corner of the NSM. This increases tensile stresses near the SSM which promotes rift initiation in the margin and propagation northwards, forming $\mathbf{C}_{2018}$. In models, loss of buttressing along a single margin increases strain rates about the opposite margin (Fig 4b). Increased strain rates about the NSM promote damage development within the margin, resulting in further weakening (Fig. S4). As the NSM begins to weaken, ice velocity continues to increase. After $\mathbf{C}_{2018}$, the speed up is concentrated around the NSM (Fig 3b).

The ice accelerates at approximately 1 m/yr/day after $\mathbf{C}_{2020}$, which removes a portion of ice that was grounded near Evans Knoll and provided critical lateral compression to the ice shelf. Ice acceleration peaks at a rate of 1.4 m/yr/day 60 days after calving. After $\mathbf{C}_{2020}$, the NSM fractures and turns into melange over the course of a year (Fig. 1c), similarly to the breakup of the SSM following $\mathbf{C}_{2017}$. After 2020, the majority of the ice shelf shifts to a tensile regime defined as $\dot{\epsilon}_2 > 0$ (Fig. 2a_3,b_3,d), which we are only able to replicate in models when removing buttressing from both margins (Fig. 4c_3). Additionally, the speed up once again originates from the NSM (Fig. 3c). After $\mathbf{C}_{2020}$, no further calving events have occurred as of January 2026, and the speed of the ice shelf has stabilized at around 4.9 km/yr.

This timeline leaves several outstanding questions.

What portion of each margin has lost the ability to support the shear stresses that provide buttressing? The

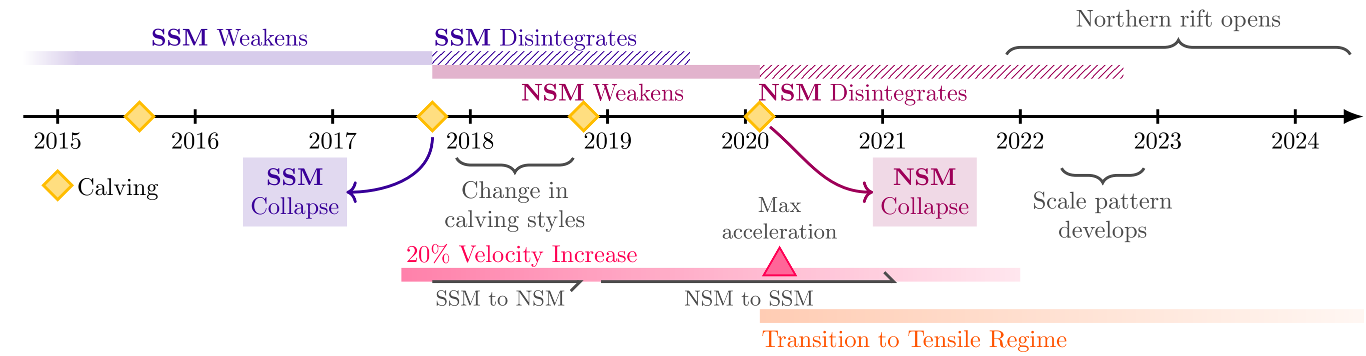

Fig. 5. Proposed timeline of buttressing loss on PIIS

SSM appears visually damaged along its entire length, but portions of the NSM do not appear as damaged. Given that the velocity of the ice shelf has somewhat stabilized from 2022 onwards, portions of each margin may still be providing some buttressing force, although we are unable to resolve where buttressing still exists with our data due to limited resolution and signal-to-noise. Recent work suggests the observed slow down of the main PIIS trunk in 2022 was the result of ephemeral coupling of the main PIIS trunk to the Southern ice shelf via dense melange left behind by the disintegration of the SSM (44). When the melange evacuates from the former SSM, velocities begin to increase again and continue to increase through the end of our observational data. This further highlights the crucial role lateral buttressing plays in stabilizing ice shelves.

How did this process of buttressing loss initiate? Due to the continuous history of change over PIIS and the limited observational record prior to the launch of Sentinel-1, it is difficult to fully disentangle when this process initiated, although these limited observations can give us insight into some of the processes involved. Damage was already present in the SSM prior to 2014. Bindschadler (31) notes that a cyclical pattern of shear margin damage development followed by calving front retreat has occurred since the 1970's, and we theorize the loss of buttressing from 2015-2024 is part of this larger pattern of retreat. Past a certain threshold, ice transitions from flowing over a pinning point to fracturing over it (28), and once that transition occurs, calving front retreat inevitably follows. A key mechanism to this process of damage production is potentially related to the increase of strain rates about the undamaged margin after one margin loses buttressing. The processes we are seeing on PIIS today could be the result of margin weakening bouncing from side to side, almost unzipping the margins of the ice shelf. Further work is needed to explore when the transition from flow to fracture occurs, as this appears to be a crucial component of understanding future buttressing loss.

Implications for the Stability of Pine Island Glacier

We present a timeline of observed loss of buttressing on Pine Island Ice Shelf over the course of a decade. Ice shelf buttressing sets the stability of PIG and its loss portends a period of irreversible ice loss and subsequent sea level rise (2, 3, 45). The rate at which PIG will now contribute to sea level rise is a source of deep uncertainty (13) and depends on a variety of factors, including ocean-driven melting (46), the mechanics and hydrology of the glacier bed (47), and the viscosity of ice (48, 49). The total loss and contribution to sea-level rise has been estimated in previous work that evaluates tipping points and early warning indicators (50). These authors identify three grounding line positions as tipping points, beyond which ice loss becomes self-sustaining until the grounding line reaches another point of stability. The current grounding line position approximates one of the tipping point positions, and we hypothesize that the grounding line will retreat in response to the loss of buttressing. As of this writing, there is no definitive evidence that such a retreat has begun, likely due to the mechanical properties and topography of the bed near the grounding zone (51). Continued observations of grounding line migration will yield further insights into the processes that set the persistence of grounding line positions in PIG.

While the future of PIG is unclear, there are some notable observations that may elucidate how PIIS will evolve. The current ice front has developed a scale-like texture which is very similar to the texture of the Thwaites Eastern Ice Tongue prior to its eventual disintegration (Fig 6b,c), and also resembles patterns present on other ice tongues across Antarctica. This pattern has likely developed due to necking of the ice as a result of viscous thinning and melt water channelization under the ice shelf, but the length scale of these features may give us insights into a material property of ice. Additionally, we note a rift growing near the grounding line of the NSM (Fig. 6a). If this rift continues to grow across the ice shelf, we may see a significant loss of ice shelf area within the next decade.

Supporting Information Appendix (SI). Additional figures of observations are provided in the Supporting Information Appendix. We provide four videos showing the evolution of ΔV, $\Delta\dot{\epsilon}_E$, $\dot{\epsilon}_E$, and $\dot{\epsilon}_2$ between 2015 and 2024.

Materials and Methods

0.1. Velocity Fields. We interpolate velocity products processed by the Greenland Ice Mapping Project (52) by fitting the velocity time series on a pixel-by-pixel basis with a collection of integrated B-splines (53). This approach allows for flexible reconstruction of temporal variations with timescales ranging from half a year to two years. Once fitted, we evaluate the B-splines on a uniformly spaced time grid to create 1000 time-dependent velocity fields over PIG from January 2015 to February 2024.

From the velocity fields, we derive strain rates as the symmetrical component of the horizontal velocity gradient tensor, which we compute at each pixel using a 4th-order Savtizky-Golay filter with a window size of

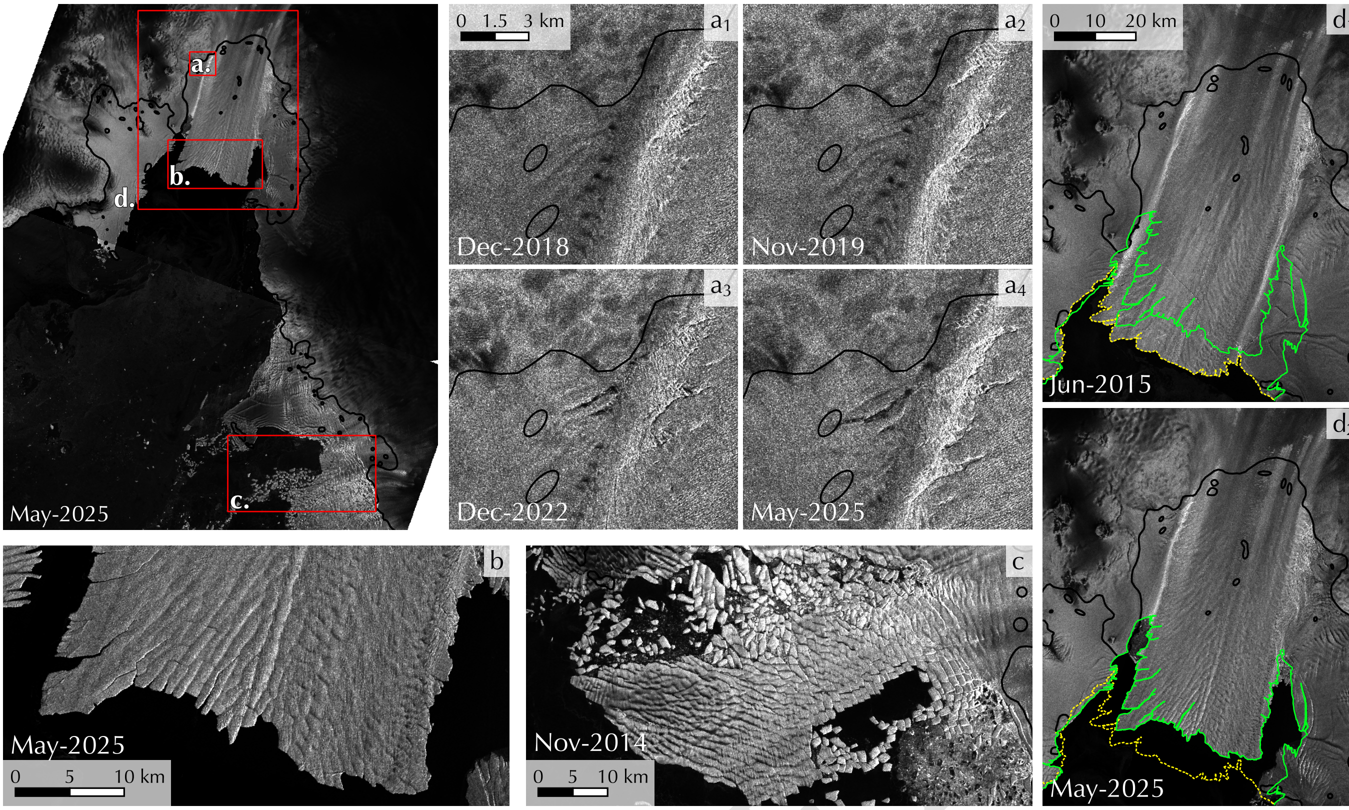

Fig. 6. (a) The evolution of a new rift close to the grounding line in the NSM, which could contribute to the next calving event on PIIS. (b) A distinctive scale-like pattern has developed on the PIIS after the disintegration of both shear margins, which resembles the pattern observed on the (c) Thwaites Western Ice Tongue prior to breakup. (d) The 2015 calving front (dashed yellow line) and the 2025 calving front (solid green line) overlain on (d$_1$) 2015 and (d$_2$) 2025 Sentinel imagery, showing the rotation of the PIIS trunk after the loss of contact with the Southern ice shelf. Contains modified Copernicus Sentinel-1 imagery

2.5 km. This window size was chosen to prioritize preservation of strain rate magnitudes and spatial patterns while minimizing the influence of velocity noise. From the strain rate tensor at each location, we calculate the principal horizontal strain rates from the tensor eigenvalues, as well as the effective strain rate computed as the square root of the second tensor invariant $\dot{\epsilon}_E = \sqrt{(\dot{\epsilon}_1^2 + \dot{\epsilon}_2^2)/2}$.

0.2. Model Setup. We implement the third phase of the Marine Ice Sheet Model Intercomparison Project (MISMIP+) (43) in the Ice-sheet and Sea-level System Model (ISSM) (42). MISMIP+ explicitly accounts for lateral buttressing which is not incorporated in MISMIP or MISMIP3d, the first two phases of the MISMIP experiments (54). The MISMIP+ model domain is 680 km along flow and 80 km across flow, and uses the Shallow Shelf Approximation (55) to simplify and solve the Stokes Equations, which averages values with depth, resulting in a 2 dimensional model. We run the model forwards on a uniform mesh for 20,000 years to achieve steady state, then refine the mesh around the grounding line and ice shelf using ISSM grid refinement functions. In steady state, our model grounding line falls approximately 440 km from the start of the model domain.

In continuum models, damage of all scales is represented as a state variable, D, that ranges from 0 (undamaged) to 1 (most damaged) and modifies the bulk viscosity of the material (37, 38, 56). Material properties are linked to flow properties within the Full Stokes Equations through constitutive relations. Ice is a non-Newtonian fluid that is well-approximated using Glen's Flow Law (57):

$$\tau_{ij} = 2\eta\dot{\epsilon}_{ij}, \quad [1]$$

where τ_{ij} is the deviatoric stress tensor, $\dot{\epsilon}_{ij}$ is the strain rate tensor, and η is the dynamic viscosity, defined as:

$$\eta_{damage} = (1 - D)\frac{B}{2\dot{\epsilon}_e^{(n-1)/n}}, \quad [2]$$

where D is the damage state variable, B is the ice rigidity (equivalent to $B = A^{-1/n}$), $\dot{\epsilon}_e$ is the effective strain rate, and n is the flow law exponent. In this work, we assume $n = 3$ for consistency with other MISMIP+ experiments.

Due to model constraints and to simplify computation, we choose to modify the value of ice rigidity, B, to simulate decreases in viscosity related to damage rather than implementing an evolving state damage variable D. We utilize an empirically-derived value of $B_{intact} = (6.338 \times 10^{-25})^{-1/3} = 1.164 \times 10^8$ Pa s$^{1/3}$ for the general ice shelf, consistent with the MISMIP+ methodology (43), and an arbitrarily chosen value of $B_{damage} = 2.0 \times 10^7$ Pa s$^{1/3}$ for the damaged shear margins, corresponding to a value of $D \approx 0.9$.

From the steady state model, we set $B = B_{damage}$ within the shear margins (highlighted in green on Fig 4) and calculate the instantaneous stress response of the model to this change in buttressing. We do not run the model forward after perturbation due to the relatively quick timescale over which the observed changes occur and due to uncertainties involved with modeling transient properties such as ice thickness, damage evolution, and grounding line migration (58). We also do not prescribe a basal melt rate since we do not run the model forward after reaching steady state. We focus entirely on changes within the buttressed floating ice shelf, as the Shallow Shelf Approximation makes assumptions that do not well-approximate grounded ice.

Data, Materials, and Software Availability. Derived velocity and strain rate data are currently being uploaded to a public repository and will be shared upon publication. Calving front traces are also being uploaded to a public repository and will be shared upon publication. All software used in this analysis are available through their referenced sources.

ACKNOWLEDGMENTS. This material is based upon work supported by the National Science Foundation Graduate Research Fellowship Program under Grant No. 2140001. Any opinions, findings, and conclusions or recommendations expressed in this material are those of the author(s) and do not necessarily reflect the views of the National Science Foundation.

SWM and BM received funding through NSF-NERC award 1853918, the John W. Jarve (1978) Seed Fund at MIT, and the NEC Corporation Fund for Research in Computers and Communications at MIT.

1. JJ Fürst, et al., The safety band of Antarctic ice shelves. *Nat. Clim. Chang.* **6**, 479–482 (2016).
2. GH Gudmundsson, Ice-shelf buttressing and the stability of marine ice sheets. *The Cryosphere* **7**, 647–655 (2013).
3. SS Pegler, Marine ice sheet dynamics: the impacts of ice-shelf buttressing. *J. Fluid Mech.* **857**, 605–647 (2018).
4. TA Scambos, JA Bohlander, CA Shuman, P Skvarca, Glacier acceleration and thinning after ice shelf collapse in the Larsen B embayment, Antarctica. *Geophys. Res. Lett.* **31** (2004) _eprint: https://onlinelibrary.wiley.com/doi/pdf/10.1029/2004GL020670.
5. H Rott, F Müller, T Nagler, D Floricioiu, The imbalance of glaciers after disintegration of Larsen-B ice shelf, Antarctic Peninsula. *The Cryosphere* **5**, 125–134 (2011).
6. A Khazendar, CP Borstad, B Scheuchl, E Rignot, H Seroussi, The evolving instability of the remnant Larsen B Ice Shelf and its tributary glaciers. *Earth Planet. Sci. Lett.* **419**, 199–210 (2015).
7. E Rignot, et al., Four decades of Antarctic Ice Sheet mass balance from 1979–2017. *Proc. Natl. Acad. Sci.* **116**, 1095–1103 (2019) _eprint: https://www.pnas.org/doi/pdf/10.1073/pnas.1812883116.
8. C Schoof, Ice sheet grounding line dynamics: Steady states, stability, and hysteresis. *J. Geophys. Res. Earth Surf.* **112** (2007) _eprint: https://onlinelibrary.wiley.com/doi/pdf/10.1029/2006JF000664.
9. CSM Doake, DG Vaughan, Rapid disintegration of the Wordie Ice Shelf in response to atmospheric warming. *Nature* **350**, 328–330 (1991).
10. DI Benn, et al., Rapid fragmentation of Thwaites Eastern Ice Shelf, West Antarctica. *Cryosphere Discuss.* **16**, 2545–2564 (2021).
11. T Scambos, C Hulbe, M Fahnestock, Climate-Induced Ice Shelf Disintegration in the Antarctic Peninsula in *Antarctic Peninsula Climate Variability: Historical and Paleoenvironmental Perspectives*, Antarctic Research Series, eds. E Domack, A Levente, A Burnet, R Bindschadler, P Convey. (American Geophysical Union (AGU)) Vol. 79, pp. 79–92 (2003) _eprint: https://onlinelibrary.wiley.com/doi/pdf/10.1029/AR079p0079.
12. TL Edwards, et al., Projected land ice contributions to twenty-first-century sea level rise. *Nature* **593**, 74–82 (2021).
13. M Oppenheimer, et al., Sea Level Rise and Implications for Low-Lying Islands, Coasts and Communities. *Camb. Univ. Press.* **IPCC Special Report on the Ocean and Cryosphere in a Changing Climate**, 321–445 (2019).
14. E Rignot, Changes in West Antarctic ice stream dynamics observed with ALOS PALSAR data. *Geophys. Res. Lett.* **35** (2008) _eprint: https://agupubs.onlinelibrary.wiley.com/doi/pdf/10.1029/2008GL033365.
15. A Shepherd, et al., A Reconciled Estimate of Ice-Sheet Mass Balance. *Science* **338**, 1183–1189 (2012).
16. JA Church, NJ White, Sea-Level Rise from the Late 19th to the Early 21st Century. *Surv. Geophys.* **32**, 585–602 (2011).
17. M Morlighem, et al., Deep glacial troughs and stabilizing ridges unveiled beneath the margins of the Antarctic ice sheet. *Nat. Geosci.* **13**, 132–137 (2020) Bandiera_abtest: a Cg_type: Nature Research Journals Number: 2 Primary_atype: Research Subject_term: Cryospheric science;Geomorphology;Projection and prediction Subject_term_id: cryospheric-science;geomorphology;projection-and-prediction.
18. RD Crabtree, CSM Doake, Pine Island Glacier and Its Drainage Basin: Results From Radio Echo-Sounding. *Annals Glaciol.* **3**, 65–70 (1982).
19. J Mouginot, E Rignot, B Scheuchl, Sustained increase in ice discharge from the Amundsen Sea Embayment, West Antarctica, from 1973 to 2013. *Geophys. Res. Lett.* **41**, 1576–1584 (2014) _eprint: https://agupubs.onlinelibrary.wiley.com/doi/pdf/10.1002/2013GL059069.
20. I Joughin, D Shapero, B Smith, P Dutrieux, M Barham, Ice-shelf retreat drives recent Pine Island Glacier speedup. *Sci. Adv.* **7**, eabg3080 (2021).
21. E Rignot, J Mouginot, M Morlighem, H Seroussi, B Scheuchl, Widespread, rapid grounding line retreat of Pine Island, Thwaites, Smith, and Kohler glaciers, West Antarctica, from 1992 to 2011. *Geophys. Res. Lett.* **41**, 3502–3509 (2014) _eprint: https://onlinelibrary.wiley.com/doi/pdf/10.1002/2014GL060140.
22. H Konrad, et al., Net retreat of Antarctic glacier grounding lines. *Nat. Geosci.* **11**, 258–262 (2018) Number: 4.
23. JW Park, et al., Sustained retreat of the Pine Island Glacier. *Geophys. Res. Lett.* **40**, 2137–2142 (2013).
24. EJ Rignot, Fast Recession of a West Antarctic Glacier. *Science* **281**, 549–551 (1998).
25. SS Jacobs, HH Hellmer, A Jenkins, Antarctic Ice Sheet melting in the southeast Pacific. *Geophys. Res. Lett.* **23**, 957–960 (1996).
26. S Jeong, IM Howat, JN Bassis, Accelerated ice shelf rifting and retreat at Pine Island Glacier, West Antarctica. *Geophys. Res. Lett.* **43**, 11,720–11,725 (2016) _eprint: https://onlinelibrary.wiley.com/doi/pdf/10.1002/2016GL071360.
27. S Sun, GH Gudmundsson, The speedup of Pine Island Ice Shelf between 2017 and 2020: revaluating the importance of ice damage. *J. Glaciol.* **69**, 1–9 (2023).
28. S Lhermitte, et al., Damage accelerates ice shelf instability and mass loss in Amundsen Sea Embayment. *Proc. Natl. Acad. Sci.* **117**, 24735–24741 (2020) _eprint: https://www.pnas.org/doi/pdf/10.1073/pnas.1912890117.
29. E Rignot, J. Mouginot, B. Scheuchl, MEaSUREs InSAR-Based Antarctica Ice Velocity Map, Version 2 (2017).
30. E Savidge, et al., Deteriorating Structural Integrity of Pine Island Glaciers Southern Ice Shelf (2017–23) Identified with Satellite-Derived Surface Deformation, Ice Velocity, and Strain Rates. *J. Glaciol.* **71**, 1–21 (2025).
31. RA Bindschadler, History of lower Pine Island Glacier, West Antarctica, from Landsat imagery. *J. Glaciol.* **48**, 536–544 (2002).
32. S Wells-Moran, M Ranganathan, B Minchew, Fracture criteria and tensile strength for natural glacier ice calibrated from remote sensing observations of Antarctic ice shelves. *J. Glaciol.* **71**, e47 (2025).
33. DG Vaughan, Relating the occurrence of crevasses to surface strain rates. *J. Glaciol.* **39**, 255–266 (1993).
34. C Borstad, D McGrath, A Pope, Fracture propagation and stability of ice shelves governed by ice shelf heterogeneity. *Geophys. Res. Lett.* **44**, 4186–4194 (2017) _eprint: https://onlinelibrary.wiley.com/doi/pdf/10.1002/2017GL072648.
35. M Izeboud, B Wouters, S de Roda Husman, S Lhermitte, Damage development on Antarctic ice shelves sensitive to climate warming. *Nat. Clim. Chang.* **15**, 1333–1339 (2025).
36. A Pralong, M Funk, Dynamic damage model of crevasse opening and application to glacier calving. *J. Geophys. Res. Solid Earth* **110** (2005) _eprint: https://onlinelibrary.wiley.com/doi/pdf/10.1029/2004JB003104.
37. R Duddu, S Jiménez, J Bassis, A non-local continuum poro-damage mechanics model for hydrofracturing of surface crevasses in grounded glaciers. *J. Glaciol.* **66**, 415–429 (2020).
38. T Albrecht, A Levermann, Fracture field for large-scale ice dynamics. *J. Glaciol.* **58**, 165–176 (2012).
39. NB Coffey, et al., Theoretical stability of ice shelf basal crevasses with a vertical temperature profile. *J. Glaciol.* **70**, e64 (2024).
40. G Moholdt, H Pritchard, J Maton, British Antarctic Survey, RINGS/Bedmap3 grounding line of the Antarctic Ice Sheet (2025).
41. K Matsuoka, et al., Towards an improved understanding of the Antarctic coastal zone and its contribution to future global sea level (2025).
42. E Larour, H Seroussi, M Morlighem, E Rignot, Continental scale, high order, high spatial resolution, ice sheet modeling using the Ice Sheet System Model (ISSM). *J. Geophys. Res. Earth Surf.* **117** (2012) _eprint: https://onlinelibrary.wiley.com/doi/pdf/10.1029/2011JF002140.
43. XS Asay-Davis, et al., Experimental design for three interrelated marine ice sheet and ocean model intercomparison projects: MISMIP v. 3 (MISMIP +), ISOMIP v. 2 (ISOMIP +) and MISOMIP v. 1 (MISOMIP1). *Geosci. Model. Dev.* **9**, 2471–2497 (2016).
44. Y Chien, C Zhou, B Riel, Mélange-Driven Coupling Between the Central Pine Island Ice Shelf and the Piglet Glacier Reverses Recent Acceleration Trends. *Geophys. Res. Lett.* **52**, e2025GL119556 (2025).
45. M Haseloff, OV Sergienko, The effect of buttressing on grounding line dynamics. *J. Glaciol.* **64**, 417–431 (2018).
46. J De Rydt, GH Gudmundsson, Coupled ice shelf-ocean modeling and complex grounding line retreat from a seabed ridge. *J. Geophys. Res. Earth Surf.* **121**, 865–880 (2016) _eprint: https://onlinelibrary.wiley.com/doi/pdf/10.1002/2015JF003791.
47. JM Barnes, GH Gudmundsson, The predictive power of ice sheet models and the regional sensitivity of ice loss to basal sliding parameterisations: a case study of Pine Island and Thwaites glaciers, West Antarctica. *The Cryosphere* **16**, 4291–4304 (2022).
48. B Getraer, M Morlighem, Increasing the Glen–Nye Power-Law Exponent Accelerates Ice-Loss Projections for the Amundsen Sea Embayment, West Antarctica. *Geophys. Res. Lett.* **52**, e2024GL112516 (2025) _eprint: https://agupubs.onlinelibrary.wiley.com/doi/pdf/10.1029/2024GL112516.
49. DF Martin, SB Kachuck, J Millstein, B Minchew, Projections of Sea Level Rise are Highly Sensitive to the Viscous Flow Law Parameters (2025).
50. SHR Rosier, et al., The tipping points and early warning indicators for Pine Island Glacier, West Antarctica. *The Cryosphere* **15**, 1501–1516 (2021).
51. AA Robel, C Schoof, E Tziperman, Persistence and variability of ice-stream grounding lines on retrograde bed slopes. *The Cryosphere* **10**, 1883–1896 (2016).
52. I Joughin, BE Smith, I Howat, Greenland Ice Mapping Project: ice flow velocity variation at sub-monthly to decadal timescales. *The Cryosphere* **12**, 2211–2227 (2018).
53. B Riel, B Minchew, I Joughin, Observing traveling waves in glaciers with remote sensing: new flexible time series methods and application to Sermeq Kujalleq (Jakobshavn Isbræ), Greenland. *The Cryosphere* **15**, 407–429 (2021).
54. F Pattyn, et al., Results of the Marine Ice Sheet Model Intercomparison Project, MISMIP. *The Cryosphere* **6**, 573–588 (2012).
55. DR MacAyeal, et al., An ice-shelf model test based on the Ross Ice Shelf, Antarctica. *Annals Glaciol.* **23**, 46–51 (1996).
56. S Jiménez, R Duddu, J Bassis, An updated-Lagrangian damage mechanics formulation for modeling the creeping flow and fracture of ice sheets. *Comput. Methods Appl. Mech. Eng.* **313**, 406–432 (2017).
57. JW Glen, The creep of polycrystalline ice. *Proc. Royal Soc. London. Ser. A. Math. Phys. Sci.* **228**, 519–538 (1955).
58. A Vieli, AJ Payne, Assessing the ability of numerical ice sheet models to simulate grounding line migration. *J. Geophys. Res. Earth Surf.* **110** (2005) _eprint: https://onlinelibrary.wiley.com/doi/pdf/10.1029/2004JF000202.

Supporting Information for

Near-total loss of buttressing stresses observed on Pine Island Ice Shelf, West Antarctica

Sarah Wells-Moran, Brent Minchew, and Bryan Riel

Sarah Wells-Moran.
E-mail: swellsmo@uchicago.edu

This PDF file includes:

Figs. S1 to S8
Legends for Movies S1 to S4
SI References

Other supporting materials for this manuscript include the following:

Movies S1 to S4

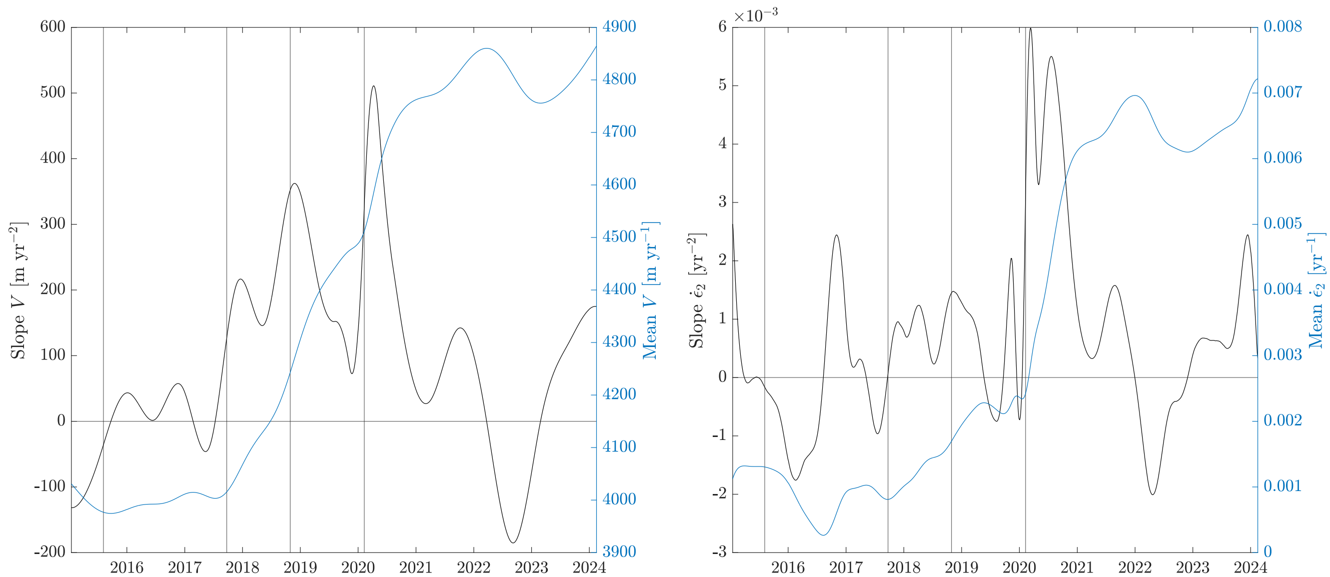

Fig. S1. The slope of mean velocity and mean least principal strain rate versus time, showing the largest slope in both data around the 2020 calving event. Velocities increase from 2017 through 2022. Least principal strain rates increase slowly after $\mathbf{C}_{2017}$ and increase by almost triple between 2020 and 2022.

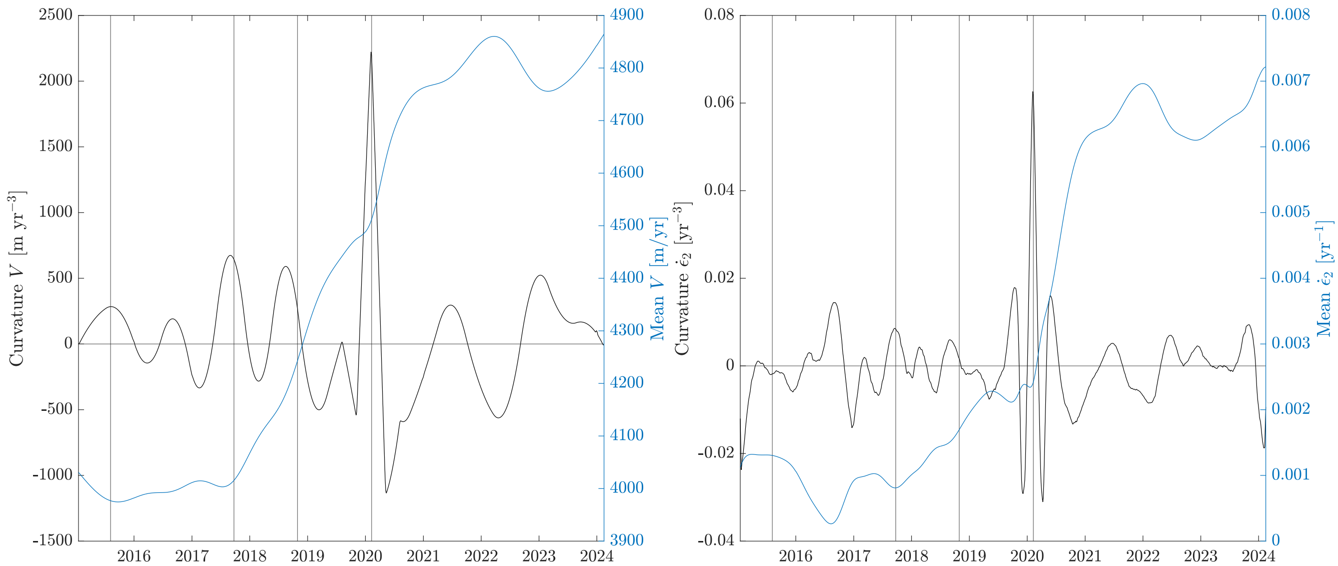

Fig. S2. The curvature of mean velocity and mean least principal strain rate versus time, showing the largest curvature in both data around the 2020 calving event. The second largest peak in curvature occurs just prior to $\mathbf{C}_{2017}$ and another similarly-sized peak occurs preceding $\mathbf{C}_{2018}$, although these peaks are similarly sized to peaks that occur in 2021 and 2023 when no calving events occur.

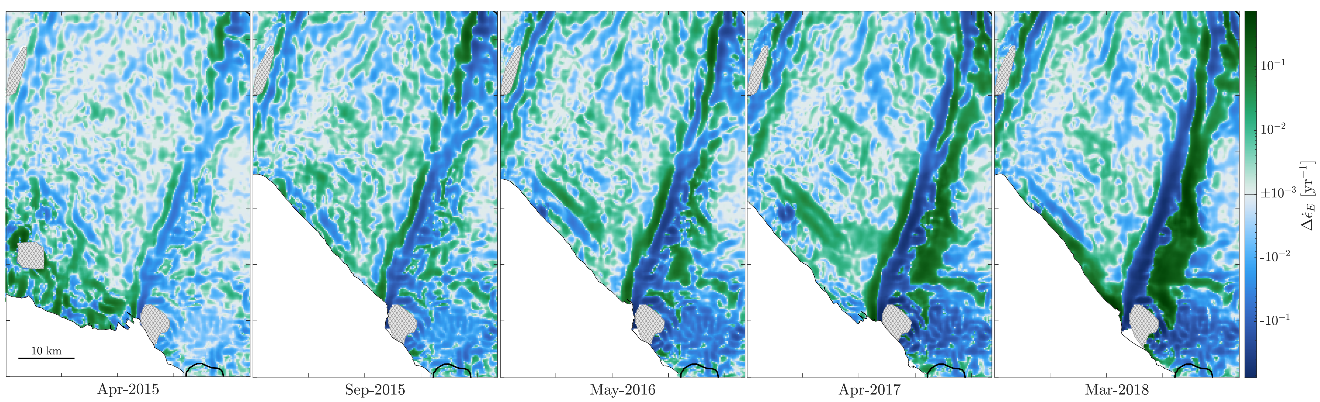

Fig. S3. Change in effective strain rates relative to January 2015 in the Southern Shear Margin. Between 2015 and 2018, the SSM migrates 5-10 km outwards from its initial location, accompanied by increasing damage and crevassing in the margin. As the margin weakens and migrates, it leaves a distinctive pattern in the $\Delta\dot{\epsilon}_E$ fields of bands of decreasing strain rates adjacent to bands of increasing strain rates. This pattern can be used to locate other regions where margins are weakening

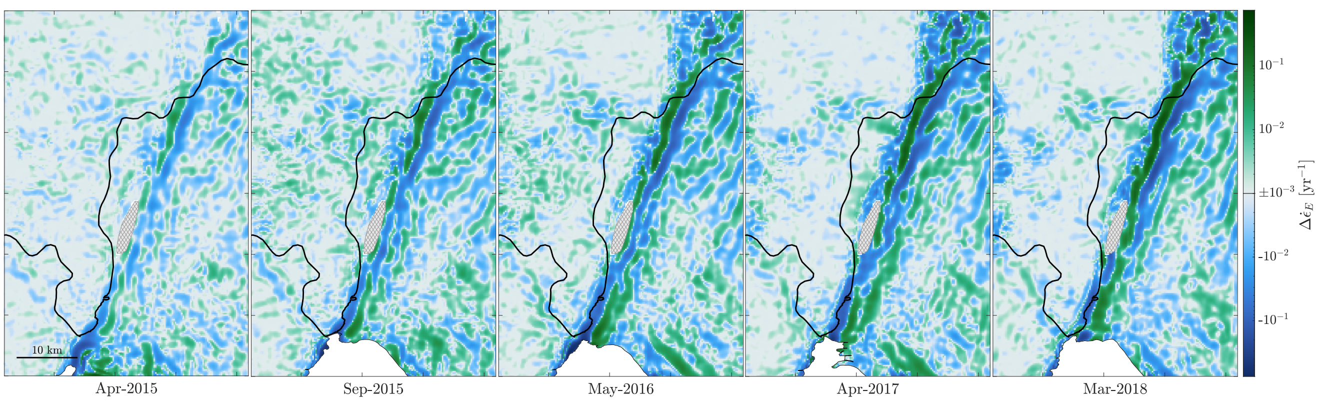

Fig. S4. Development of weakening in the NSM visualized via change in effective strain rates relative to January 2015. The pattern of margin weakening starts towards the grounding line in the NSM and advects downstream, covering the entire NSM by the end of 2018.

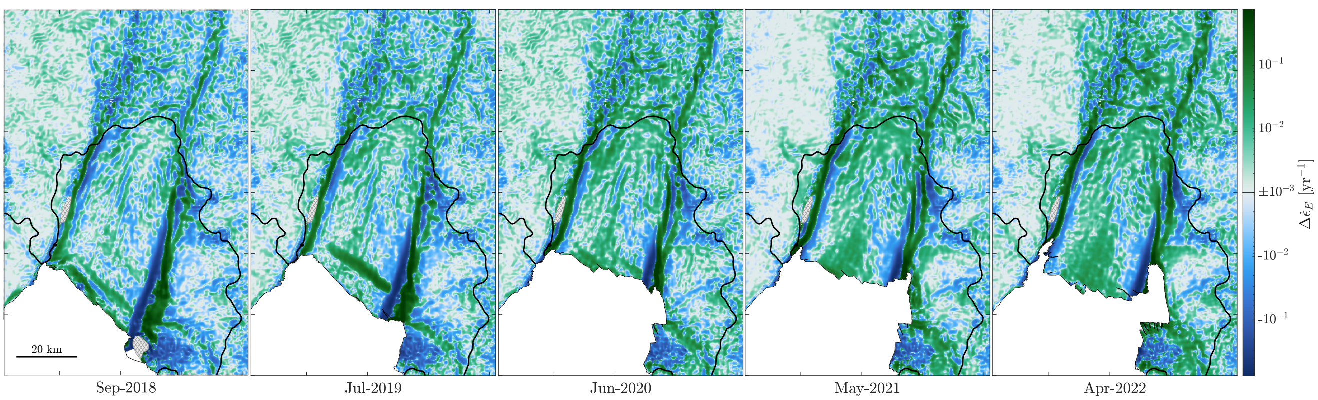

Fig. S5. Continued intensification of strain rates within both margins as the ice shelf evolves post 2018.

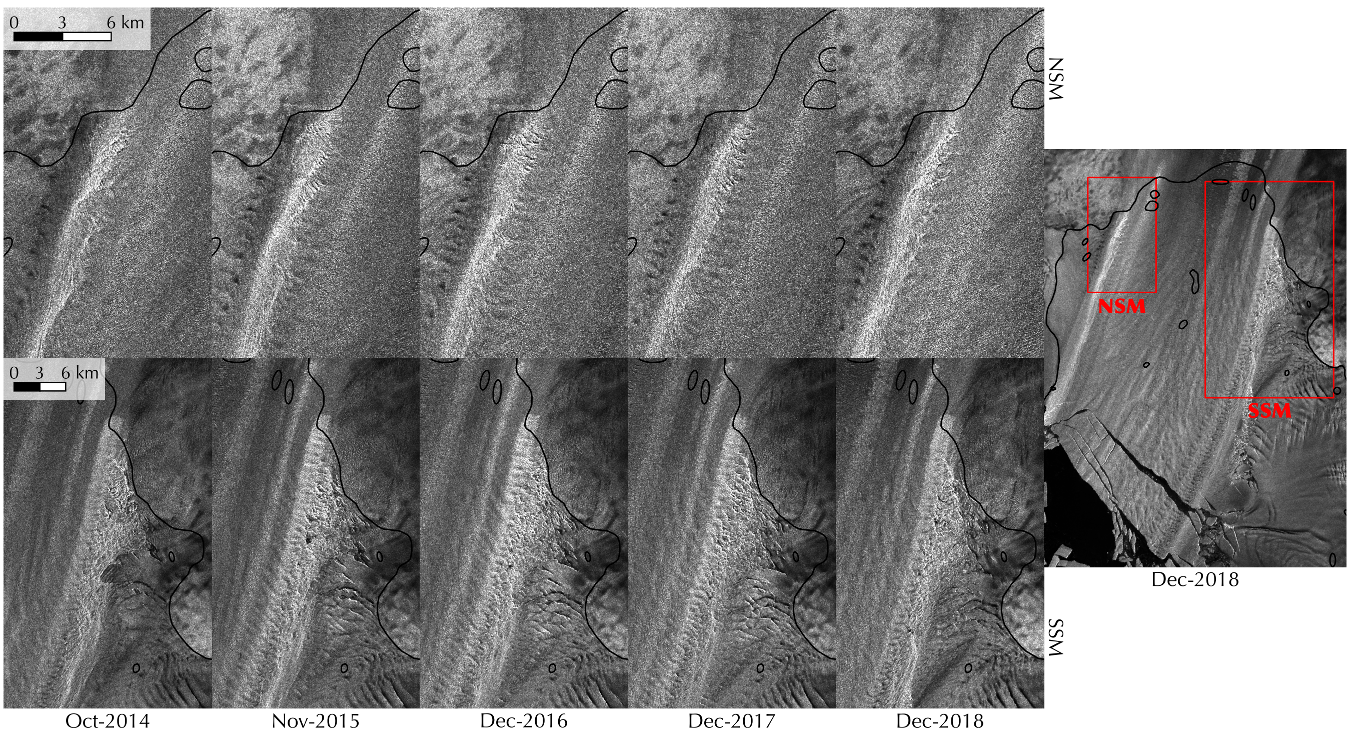

Fig. S6. Regions which generate damage near the grounding line in both the NSM (top) and SSM (bottom). The damage then advects downstream with ice flow. Damage generation within the SSM is likely to have been occurring for 5-10 years prior to 2015, as evidenced by the large area of damage downstream of the grounding line. The damage along the NSM is likely to have initiated relatively recent to 2015. Contains modified Copernicus Sentinel-1 imagery

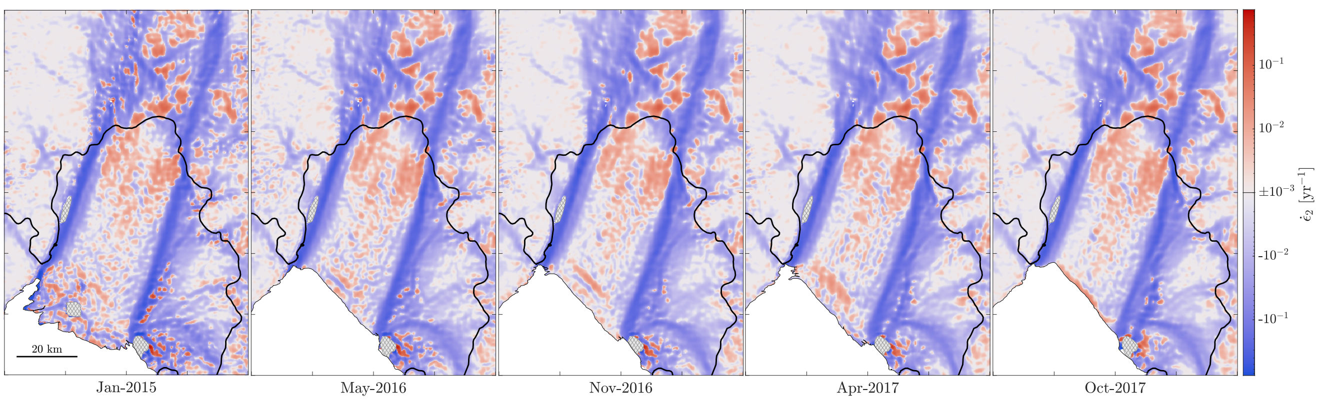

Fig. S7. $\dot{\epsilon}_2$ fields prior to loss of buttressing

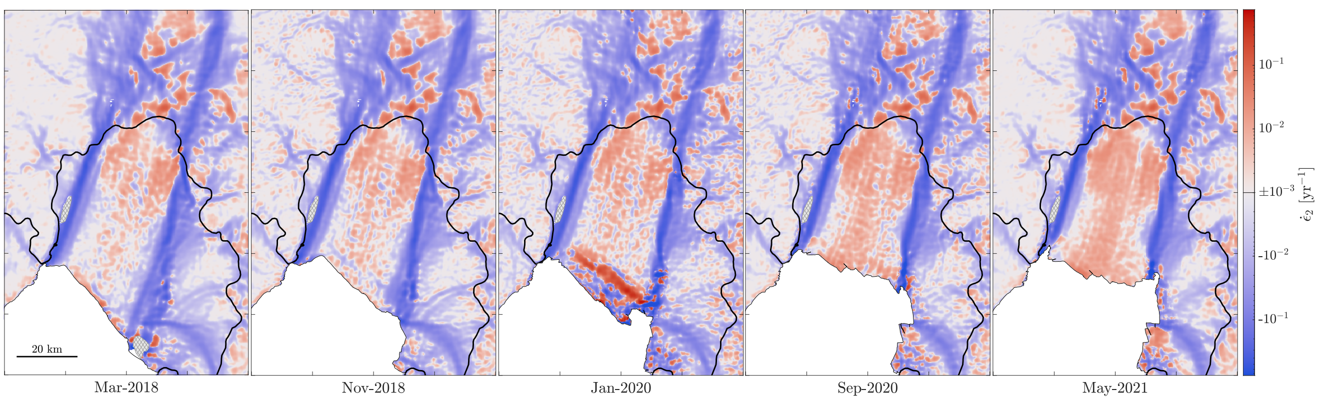

Fig. S8. Slight increase in area of tensile regime ($\dot{\epsilon}_2 > 0$) after $\mathbf{C}_{2017}$, followed by a transition to a near-total tensile regime across the entire ice shelf after $\mathbf{C}_{2020}$

Movie S1. Change in ice velocity relative to 2015 over Pine Island Ice Shelf from 2015 to 2024. Grey represents regions where ice velocity decreases relative to 2015 values. The velocity increase initiates from the SSM after the 2017 calving event and propagates towards the NSM. After the 2018 and 2020 calving events, the velocity increase propagates from the NSM towards the SSM. The plot below the map shows velocities averaged over the black box in the center of the ice shelf, with vertical black bars denoting calving events. Calving fronts are traced by the authors from Sentinel-1 imagery. Grounding line from (1, 2)

Movie S2. Change in $\dot{\epsilon}_E$ relative to 2015 over Pine Island Ice Shelf from 2015 to 2024. Green denotes areas where $\dot{\epsilon}_E$ increases relative to 2015 and blue denotes areas where $\dot{\epsilon}_E$ decreases relative to 2015. As the margins weaken, a distinctive pattern develops of decreasing $\dot{\epsilon}_E$ just outside of the margin and increasing $\dot{\epsilon}_E$ within the margin. The plot below the map shows $\dot{\epsilon}_E$ averaged over the black box in the center of the ice shelf, with vertical black bars denoting calving events. Calving fronts are traced by the authors from Sentinel-1 imagery. Grounding line from (1, 2)

Movie S3. Evolution of $\dot{\epsilon}_E$ on Pine Island Ice Shelf from 2015 to 2024. The plot below the map shows $\dot{\epsilon}_E$ averaged over the black box in the center of the ice shelf, with vertical black bars denoting calving events. Calving fronts are traced by the authors from Sentinel-1 imagery. Grounding line from (1, 2)

Movie S4. Evolution of $\dot{\epsilon}_2$ on Pine Island Ice Shelf from 2015 to 2024. Red denotes areas of positive $\dot{\epsilon}_2$ where the ice shelf is in pure tension. After the 2020 calving event, The majority of the ice shelf transitions to a purely tensile regime. The plot below the map shows $\dot{\epsilon}_2$ averaged over the black box in the center of the ice shelf, with vertical black bars denoting calving events. Calving fronts are traced by the authors from Sentinel-1 imagery. Grounding line from (1, 2)

References

1. G Moholdt, H Pritchard, J Maton, British Antarctic Survey, RINGS/Bedmap3 grounding line of the Antarctic Ice Sheet (2025).
2. K Matsuoka, et al., Towards an improved understanding of the Antarctic coastal zone and its contribution to future global sea level (2025).